Journal of Molecular Structure 1028 (2012) 88–96

Contents lists available at SciVerse ScienceDirect

Journal of Molecular Structure

journal homepage: www.elsevier.com/locate/molstruc

Synthesis of diosgenin *p*-nitrobenzoate by Steglich method, its crystal structure and quantum chemical studies

Arun Sethi [a,*], Akriti Bhatia [a], Dolly Shukla [a], Abhinav Kumar [a], Ravi Sonker [b], Rohit Prakash [a], Gitika Bhatia [b]

[a] Department of Chemistry, University of Lucknow, Lucknow 226 007, UP, India
[b] Biochemistry Division, C.D.R.I., Lucknow 226 001, UP, India

HIGHLIGHTS

- One pot Steglich esterification of diosgenin, without opening of spiro ring in high yield.
- Stereochemistry assigned to the title compound using X-ray crystallography.
- Theoretical calculations made using DFT/B3LYP/6-31G(d,p) method.
- Chemical reactivity explained with the aid of molecular elestroscostatic potential surface.
- The title compound was screened for cytotoxicity and anti-adipogenic activity.

ARTICLE INFO

Article history:
Received 19 April 2012
Received in revised form 21 May 2012
Accepted 23 May 2012
Available online 13 June 2012

Keywords:
DFT
X-ray crystallography
Anti-adipogenic activity
HOMO and LUMO energy
GIAO method
Steglich esterification

ABSTRACT

In the present study, a novel one pot synthetic route for the synthesis of diosgenin *p*-nitrobenzoate (**2**) is described from cheap, commercially available naturally occurring sapogenin–diosgenin. The molecular geometry, IR frequencies, Gauge-including atomic orbital (GIAO), ^{1}H and ^{13}C NMR chemical shifts of compound **2** has been calculated in the ground state by using the Hartree–Fock (HF) and density functional method (DFT/B3LYP) using 6-31G(d,p) basis set. The structure of diosgenin *p*-nitrobenzoate (**2**) has been confirmed by single crystal X-ray diffraction. The compound crystallizes in monoclinic form having space group P21 with cell parameters $a = 7.719(2)$ Å, $b = 8.425(2)$ Å and $c = 22.578(6)$ Å, $\alpha = 90.00$, $\beta = 98.46$ and $\gamma = 90.00$. The oxygen atoms O5 and O4 of the nitro and carbonyl ester, respectively display weak intermolecular N1—O5···H7′ and C1′=O4···H4′ interactions having dimensions of 2.61 and 2.59 Å, respectively to form intricate 1D network. The study of the electronic properties such as HOMO and LUMO energy were performed using time dependent DFT (TD-DFT) calculations. The calculated HOMO and LUMO energy values indicate that charge transfer takes place within the molecule. The compound was screened for cytotoxicity and anti-adipogenic activity.

1. Introduction

Diosgenin (25R-Spirost-en-3β-ol) is one of the most important steroidal sapogenin, which is widely used in the pharmaceutical industry as a precursor for the synthesis of a number of steroidal drugs like progesterone [1] and cortisone [2]. In recent years, there have been many reports on the important pharmacological attributes of diosgenin such as anti-cancer activity, antagonistic effect on rheumatoid arthritis, anti-malarial and anti-proliferative property [3–6]. Several reports have shown that diosgenin inhibits proliferation and induces apoptosis in a wide variety of tumor cells of colon [7], osteosarcoma [8], leukemia [9], erythroleukemia [10], breast [11], and liver [12]. Studies have proved that diosgenin can be absorbed through the gut and plays an important role in the control of cholesterol metabolism [13]. Preclinical studies have also demonstrated diosgenin efficacy against hyperglycemia, hypercholesterolemia and hypertriacylglycerolemia [14–16]. As part of our programme for synthesis of some biologically active steroidal derivatives [17,18], one pot synthesis of a new biologically active diosgenin derivative (**2**) is herein reported. A typical procedure to synthesize esters is the Fischer esterification, where in a carboxylic acid is treated with an alcohol in the presence of a mineral acid catalyst. Diosgenin when subjected to Fishers esterification usually leads to the formation of three compounds (as verified by TLC) which probably may be due to Spiro ring cleavage, resulting in the formation of side products, as the spiroketal ring is highly sensitive towards acidic conditions and readily undergoes

* Corresponding author. Tel.: +91 9415396239.
E-mail address: alkaarunsethi@rediffmail.com (A. Sethi).

0022-2860/$ - see front matter © 2012 Elsevier B.V. All rights reserved.
http://dx.doi.org/10.1016/j.molstruc.2012.05.057

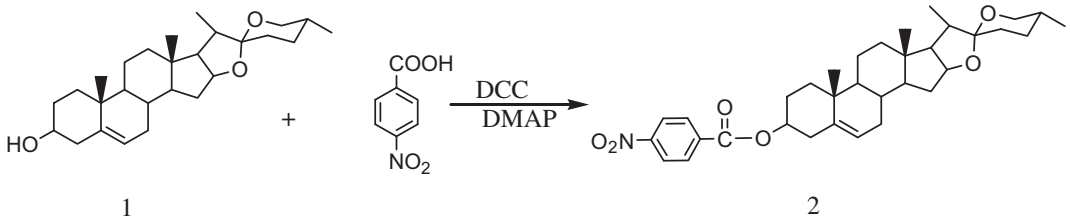

1 2

Scheme 1.

ring opening process. However, in our newly adopted experimental protocol, Steglich esterification of diosgenin was carried out using *N*,*N*′-Dicylcohexylcarbodiimide (DCC) as a coupling reagent and 4-Dimethylaminopyridine (DMAP) as a catalyst (Scheme 1) [19]. The structure of the desired compound diosgenin *p*-nitrobenzoate (**2**) in which the Spiro ring is intact, is well interpreted with the help of ^{1}H, ^{13}C, 2D (^{1}H—^{1}H COSY) NMR, IR and UV–Vis spectroscopy. In order to provide additional proof, and to investigate the stereochemistry and crystal packing of molecule, single crystal X-ray diffraction analysis was also performed. Further in order to get a better knowledge of the reactivity of the synthesized compound, theoretical studies by Hartree–Fock (HF) and density functional method (DFT/B3LYP) were also carried out. In addition, HOMO and LUMO analysis have been carried out to elucidate the information regarding charge transfer within the molecule.

2. Experimental section

2.1. Material and measurements

All reagents used for synthesis were purchased from Sigma Aldrich (St. Louis, MO) and used without further purification. IR spectra was recorded in KBr disk on a Nicolet MX-1 FTIR spectrophotometer, ^{1}H NMR spectra was recorded in $CDCl_3$ solvent on a Bruker DRX-300 MHz spectrometer, 2D (^{1}H—^{1}H COSY) NMR spectra was recorded on 600 MHz Varian Inova spectrometer, whereas ^{13}C NMR was recorded on 150 MHz Varian Inova spectrometer using $CDCl_3$ as the solvent where the chemical shifts were reported in parts per million (ppm) units with respect to TMS as internal standard. Melting point was determined using open capillary tube method and is uncorrected. The compound was purified by column chromatography and the purity of the compound was checked by TLC. Cell culture media and supplements were purchased from Invitrogen (Carlsbad, CA).

2.2. Synthesis of Diosgenin p-nitrobenzoate (DPNB)

A solution of *p*-nitrobenzoic acid (0.25 g, 1.5 mmol), DCC (0.20 g, 1.0 mmol), DMAP (0.18 g, 1.5 mmol) and diosgenin (0.62 g, 1.5 mmol) in toluene (20 mL) was stirred mechanically at room temperature until reaction was complete (progress of reaction was monitored by TLC). *N*,*N*′-dicyclohexylurea formed during the reaction was filtered off and the filtrate washed successively with water, 5% HCl and water, and then dried over anhydrous sodium sulfate. Toluene was evaporated under reduced pressure and the crude product obtained was purified by column chromatography using ethyl acetate–hexane (5%) as eluent (Yield 0.58 g, 95%). Slow evaporation of ethyl acetate during recrystallization yielded colorless needle-shaped crystals of compound **2**. m.p: 218 °C. ^{1}H NMR ($CDCl_3$, 300 MHz) δ (ppm) 8.272 (2*H*, d, Ar —H, J = 6 Hz), 8.221 (2*H*, d, Ar—H, J = 6 Hz), 5.447 (1*H*, m, H-6), 4.933–4.885 (1*H*, m, H-3), 4.460–4.389 (1*H*, m, H-16), 3.499–3.345 (2*H*, m, H-26), 2.503 (2*H*, d, H-4, J = 6 Hz), 1.313 (3*H*, s, CH_3-19), 1.293 (3*H*, s, CH_3-18), 0.96 (3*H*, d, CH_3-21 J = 6 Hz), 0.78 (3*H*, d, CH_3-27, J = 6 Hz); ^{13}C NMR (150 MHz, $CDCl_3$) δ (ppm) 164.06(C-1′), 150.44(C-5′), 139.28(C-5), 136.18(C-2′), 130.65(C-3′ and C-7′), 123.45(C4′ and C-6′), 122.909(C-6), 109.283(C-22), 80.787(C-3), 5.705(C-26), 66.848(C-16), 62.087(C-17), 56.426(C-9), 49.941(C-14), 41.617(C-4), 40.266(C-10), 39.709(C-20), 38.069(C-13), 36.925(C-23), 36.772(C-2), 32.065(C-1), 31.843(C-12), 31.408(C-7), 31.386(C-25), 30.295(C-8), 28.807(C-15), 27.769(C-24), 20.842(C-11), 19.369(C-18), 17.134(C-19), 16.287(C-27), 14.524(C-21).

2.2.1. Crystal structure determination and refinement

Intensity data for the colorless crystals of the compound **2** was collected at 100(2) K on a Bruker SMART diffractometer system equipped with graphite monochromated Mo Kα radiation λ = 0.71073 Å. The final unit cell determination, scaling of the data, and corrections for Lorentz and polarization effects were performed with Bruker SAINT [20]. A symmetry-related (multi-scan) absorption correction has been applied. Structure solution, followed by full-matrix least squares refinement was performed using the WINGX-1.70 suite [21] of programs throughout. The structure was solved by direct methods SHELXS97 [22] and crystal refinement was done using SHELXL97 [22]. All non-hydrogen atoms were refined anisotropically; hydrogen atoms were located at calculated positions and refined using a riding model with isotropic thermal parameters fixed at 1.2 times the Ueq value of the appropriate carrier atom. The conformations of the ring were calculated using PLATON [23]. The perspective view of the molecule

Table 1
Crystallographic data and structure refinement for compound **2**.

CCDC no.	854729
Crystal description	Colorless, plate
Empirical formula	$C_{34}H_{45}NO_6$
Formula weight (g mol^{-1})	563.71
Temperature (K)	100(2)
Crystal system	Monoclinic
Space group	P2(1)
a (Å)	7.719(2)
b (Å)	8.425(2)
c (Å)	22.578(6)
α (°)	90.00
β (°)	98.46
γ (°)	90.00
V (Å^3)	1452.3(7)
Z	2
D_{calc} (g cm^{-3})	1.289
Absorption coefficient (mm^{-1})	0.087
F(000)	608
Crystal size (mm^3)	0.35 × 0.20 × 0.15
θ (min–max) (°)	1.82–28.34
Reflections collected	9548
Independent reflections	5600 [R_{int} = 0.0525]
Data/restraints/parameters	5600/0/370
Final R indices [$I > 2\sigma(I)$]	$R1$ = 0.0641, $wR2$ = 0.1327
R indices (all data)	$R1$ = 0.0961, $wR2$ = 0.1667
Goodness-of-fit on F^2	1.061
Absolute structure parameter	−0.4(15)
Largest difference peak and hole (e Å^{-3})	0.359 and −0.368
Absolute structure parameter	−0.05(5)

was prepared using ORTEP [24]. The crystallographic data are summarized in Table 1.

2.2.2. Anti-adipogenic activity

2.2.2.1. Cell culture. Rat 3T3-L1 preadipocytes were cultured in DMEM (Dulbecco's modified Eagle's medium) supplemented with 10% (v/v) fetal bovine serum (FBS) so as to aid them to grow to confluency. Two days postconfluency, 3T3-L1 preadipocytes (day 0) were stimulated for 72 h by adding 500 μM IBMX (3-isobutyl-1-methylxantine), 1 μM dexamethasone and 1 μM insulin [MDI] to the DMEM/10%FBS culture medium in presence of compound **1** and **2** at concentrations of 5 μM and 10 μM (treatment group) as well as 0.1% DMSO (control or vehicle group) to induce differentiation of preadipocytes to adipocytes. Subsequently, on day 3, the MDI medium was replaced with DMEM/10%FBS containing 1 μM insulin. On day 5, the MDI medium was replaced with DMEM/10%FBS and refreshed at 2 days intervals thereafter until analysis was performed on day 7–10. Between day 3 and induction of differentiation (day 7–10) cells maintained in culture medium were observed daily.

2.2.2.2. Cell viability. MTT [3-(4,5-dimethylthiazol-2-yl)-2,5-diphenyltetrazolium bromide] cell proliferation and viability assay is a safe, *in vitro* assay for the measurement of cell proliferation and reduction in cell viability. The tetrazolium compound MTT was reduced by metabolically active cells to insoluble purple formazan dye crystals. Preconfluent 3T3-L1 preadipocytes were seeded in 96-well culture plates at a density of 10,000 cells/well. Compounds **1** and **2** (treatment group) as well as control group (0.1% DMSO) were added to culture medium at time of plating. After 48 h following plating, the cells were incubated with 0.5 mg/mL MTT for 45 min. The medium was aspirated and the insoluble formazan product was dissolved in DMSO (150 μL) for at least 2 h in the dark. MTT reduction was quantified by measuring the absorbance at 550 nm. Both control/treatment groups were assayed in triplicate and each experiment was repeated at least three times.

2.2.2.3. TG quantification. On day 8 following differentiation, TG concentration was determined by extracting the cells with $CHCl_3$/MEOH (2:1 v/v) as described earlier [25], separating the chloroform and methanol–water phases, removing phospholipids, and further processing the cultured cells using modified method adopted by Frayn and Maycock [26]. Triglycerides were then quantified spectrophotometrically as glycerol using an enzymatic assay kit (Sigma chemical).

2.2.2.4. Oil red O staining. 3T3-L1 adipocytes were fixed in 4% paraformaldehyde for 20 min, washed with PBS and stained with 0.34 Oil red O (Sigma, Saint Louis, MO) in 60% isopropanol for 15 min. It was washed with PBS thrice and stain was extracted with 80% isopropanol by keeping it at room temperature for 30 min and absorbance was measured at 520 nm.

2.2.3. Computational details

All calculations of the title compound **2** were carried out using Gaussian 03 program package [27] for predicting the molecular structure, vibrational wavenumbers, ^{1}H and ^{13}C NMR chemical shifts. The geometry of the molecule was optimized by density functional theory (DFT) as well as Hartree Fock (HF) level of theory using B3LYP functional and 6-31G(d,p) basis set [28]. In the vibrational frequency calculations, all stationary points were assigned minimum values using the optimized geometrical parameters and their harmonic vibrational wave numbers are positive. The vibrational frequencies in the harmonic approximation were calculated using B3LYP/6-31G(d,p). Since the calculated vibrational frequencies were higher than the experimental frequencies, they were scaled down by the single scaling factor 0.9608 [29]. The electronic properties were calculated using TD-DFT/B3LYP/6-31G(d,p) method. All molecular structures were visualized using CHEMCRAFT [30] and Gauss View [31] softwares.

3. Results and discussion

3.1. Optimized geometry and energies

Initial geometry of compound **2** was taken from the single crystal X-ray diffraction data and was optimized. The ground state optimized structure of compound **2** is presented in Fig. 1. The optimized structure and experimental structure (from single crystal X-ray) of compound **2** were compared by superimposing them using a least squares algorithm that minimizes the distances of the corresponding non-hydrogen atoms as shown in Supplementary Fig. 1. The agreement between the optimized and experimental crystal structure was quite good showing that the geometry optimization almost exactly reproduces the experimental conformation. The relative energies of the molecule were calculated employing *ab-initio* functions, HF and DFT functional (B3LYP) methods. The energy for the optimized compound **2** structure is −1817.34376 and −1828.81778 a.u. as calculated by HF and DFT level of theory respectively. However the optimized energy of the title compound at HF level of theory was found to be 11.4740 a.u. higher than the DFT level of theory.

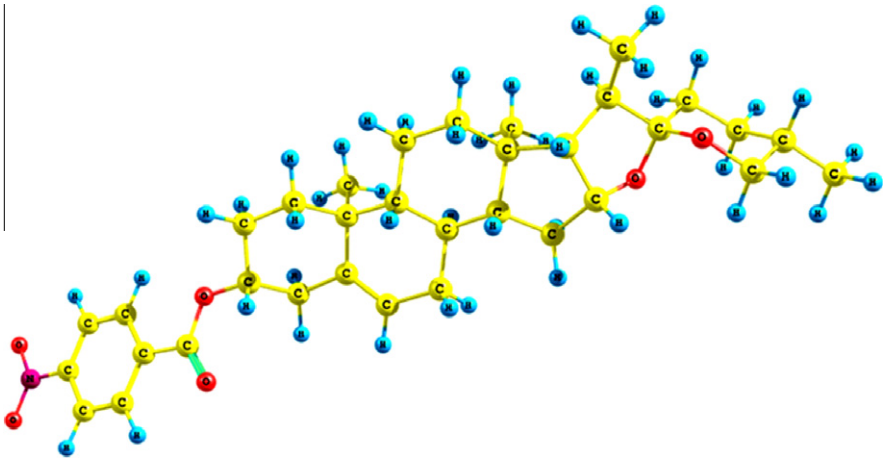

Fig. 1. Optimized geometry of compound **2** at B3LYP/6-31G(d,p) level of theory.

Table 2
Comparison between few selected experimental and optimized geometry parameters of compound **2** using B3LYP/6-31G(d,p).

Bonds	Bond lengths (X-ray)	Optimized bond (DFT)	Optimized bond (HF)
C_3—C_4	1.520(5)	1.530	1.522
C_9—C_8	1.537(5)	1.553	1.547
C_{10}—C_5	1.524(5)	1.534	1.533
C_{10}—C_9	1.550(5)	1.569	1.562
C_6—C_7	1.494(5)	1.500	1.500
C_9—C_{11}	1.540(5)	1.548	1.545
C_{14}—C_{13}	1.542(4)	1.553	1.544
C_{17}—C_{16}	1.550(5)	1.560	1.550
O_1—C_{22}	1.423(4)	1.424	1.397
C_{22}—O_2	1.424(4)	1.424	1.398
C_{20}—C_{22}	1.536(5)	1.554	1.544
C_{24}—C_{25}	1.522(6)	1.536	1.531
$C_{1'}$—$C_{2'}$	1.487(5)	1.498	1.499
Bond angle			
$C_{1'}$—O_3—C_3	118.7(3)	117.3	119.0
C_5—C_{10}—C_1	107.2(3)	107.9	107.9
C_7—C_8—C_9	108.8(3)	109.8	109.7
C_8—C_{14}—C_{13}	114.4(3)	115.0	115.1
C_{15}—C_{16}—C_{17}	107.5(3)	107.7	107.7
C_{23}—C_{22}—O_2	110.3(3)	110.7	110.4
Dihedral angle			
$C_{1'}$—O_3—C_3—C_4	−73.6(4)	85.0	83.4
C_4—C_5—C_{10}—C_9	−168.6(3)	166.1	165.9
C_7—C_8—C_9—C_{11}	−168.6(3)	170.7	170.6
C_8—C_{14}—C_{13}—C_{12}	−60.9(4)	59.5	59.3
C_{15}—C_{14}—C_{13}—C_{17}	48.8(3)	−46.8	−47.2
C_{15}—C_{16}—C_{17}—C_{20}	140.5(3)	−138.1	−137.3
C_{20}—C_{22}—C_{23}—C_{24}	−175.4(3)	173.9	174.5

The optimized molecular structure of compound **2** possesses C_1 point group symmetry. The optimized structural parameters (bond lengths, bond angles, dihedral angle) of compound **2** have been compared with those obtained experimentally from the single crystal X-ray diffraction data as shown in Table 2. It was seen that the DFT and HF methods gave comparable geometries, which differ from each other by not more than 0.037 Å/0.046 Å (DFT/HF) in bond length and 2.0°/2.0° (DFT/HF) in bond angles. The bond lengths of hydrogen atoms (C—H) show variation in our DFT and HF calculations from single crystal data (C—H). The elongated C—H bond is not only observed in our DFT and HF calculations but similar observations have been reported earlier [32].

3.2. X-ray single crystal structure

Compound **2** crystallizes in P21 space group having two molecules per unit cell. The ORTEP diagram of the compound **2** is presented in Fig. 2. The bond distances, bond angles and dihedral angles of DPNB are in good agreement with those reported for similar type of steroid molecules [33,34]. The C1—C10 bond distance in ring A is 1.555(5) Å and C9—C10 bond distance in ring B is 1.550(5) Å both corresponding to values slightly greater than other C—C bond lengths in ring A and ring B. This may be due to the presence of bridgehead methyl group at the junction of ring A and B, which relieves the strain and thus causes lengthening of C1—C10 and C9—C10 bonds.

The C22—O1 bond length 1.423 Å(4) is shorter than C16—O1 bond length 1.433 Å(4). This is probably due to the presence of two electronegative atoms, O1 and O2, with non-bonded electrons adjacent to C22. This feature has been observed in similar type of steroidal molecules [33,34].

The six membered ring A adopts a chair conformation with C1, C2, C4 and C5 atoms displaying equal deviations of 0.013 Å from their plane. However, slight deviation from the ideal chair form can be expressed by the loss of rotational symmetry through bonds C1—C2 and C4—C5 [ΔC_2 (C1—C2) = 1.6(4), (C4—C5) = 1.6(4)] with retention of the perpendicular mirror symmetry [ΔC_s (C3) = 2.4(4)]. In ring B the C5—C6 bond length of 1.329 Å(5) confirms the location of double bond, with the environment at C5 atom being planer. Due to the presence of double bond, ring B adopts an 8β-9α half-chair conformation with the rotational axis bisecting C5—C6 and C8—C9 bonds and with asymmetry parameter [ΔC_2 (C5—C6) = 0.7(4)]. Ring C on the other hand has approximately chair conformation typical for totally saturated ring. The atoms C12, C11 and C8 are deviated by 0.003 Å whereas atom C14 shows 0.004 Å deviation from the plane passing through these atoms. Marginal increase in the deviation from plane for C14 (0.004 Å) as compared to C12, C11 and C8 (0.003 Å) is because of the fact that C14 is a member of five membered ring D. Ring C therefore due to the strain at junction with five-membered D ring shows slight distortion from ideal chair form [ΔC_2 (C8—C9) = 5.1(4)], [ΔC_s (C8) = 8.0(4)].

Table 3
Endocyclic torsion angles (°) about the ring junctions of compound **2**.

Junction	Atoms	Torsion angle	Characteristics
A/B	C4—C5—C10—C1	−50.27	Quasi-trans
	C6—C5—C10—C9	11.74	
B/C	C7—C8—C9—C10	63.19	Trans
	C14—C8—C9—C11	−47.15	
C/D	C12—C13—C14—C8	−60.87	Trans
	C17—C13—C14—C15	48.74	
D/E	C13—C17—C16—C—15	14.67	Cis
	C20—C17—C16—O1	20.85	

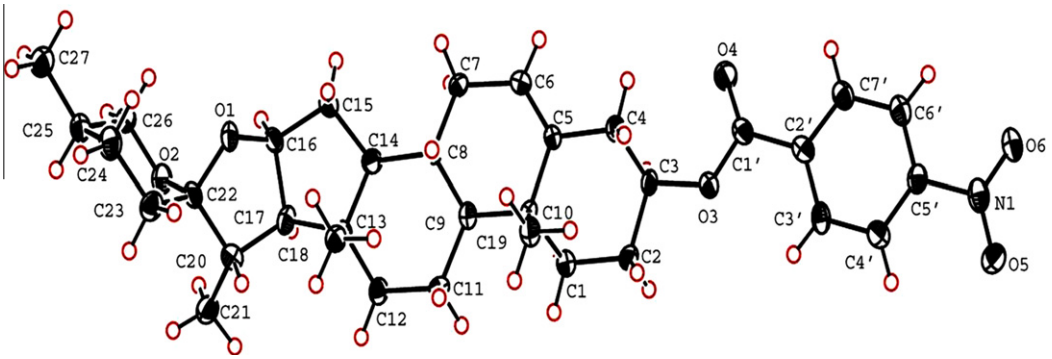

Fig. 2. ORTEP view of compound **2** with displacement ellipsoids drawn at 30% probability level.

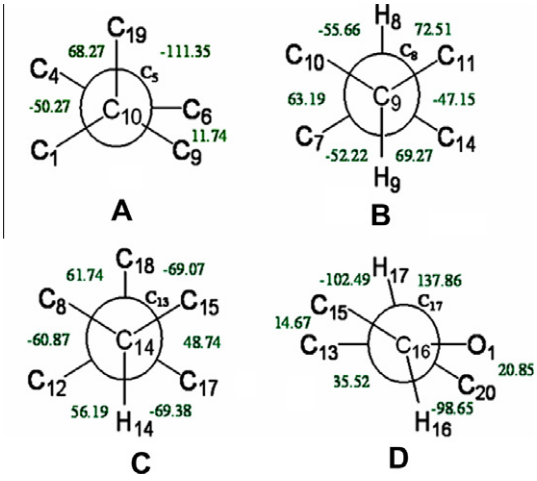

Fig. 3. Newman projections along C10—C5 (A), C9—C8 (B), C14—C13 (C) and C16—C17 (D) bonds.

Ring D adopts a 13β-14α half chair conformation [ΔC_2 (C13—C14) = 1.6(4)]. The five membered ring E[ΔC_s (O1) = 4.1(4)] has an exo O1 envelope conformation with the O1 atom showing a deviation of 0.550 from the C22—C20—C17—C16 plane and the dihedral angle between the planes C22—C20—C17—C16 and C22—O1—C16 corresponds to 39.64°. The six membered ring F acquires chair conformation with asymmetry parameters [ΔC_2 (C23—C24) = 0.5(4)], [ΔC_s (C24) = 2.2(3)], where the atoms C26, O2, C23, C24 display equal deviations of 0.009 Å from the C26—O2—C23—C24 plane. The ring junctions B/C and C/D are trans, whereas the ring junction A/B is quasi trans while D/E is cis. A list of endocyclic torsion angles given in Table 3 and Newman projections along the bonds involved in ring fusion are shown in Fig. 3.

The crystal structure of the molecule is stabilized by weak intermolecular interactions. The oxygen atoms O5 and O4 of the nitro and carbonyl ester, respectively display weak intermolecular N1—O5···H7′ and C1′=O4···H4′ interactions to form intricate 1D network (Fig. 4) The N1—O5···H7′ interaction have dimension of 2.61 Å and ∠N1—O5···H7′ is 159.35°. While in the case of C1′=O4···H4′ interaction the length is 2.59 Å and ∠C1′=O4···H4′

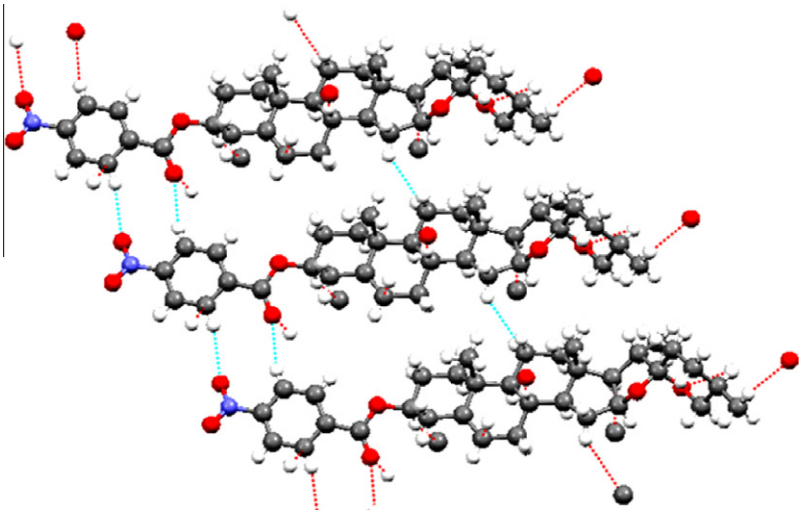

Fig. 4. Molecular chain of compound **2** showing weak intermolecular interactions.

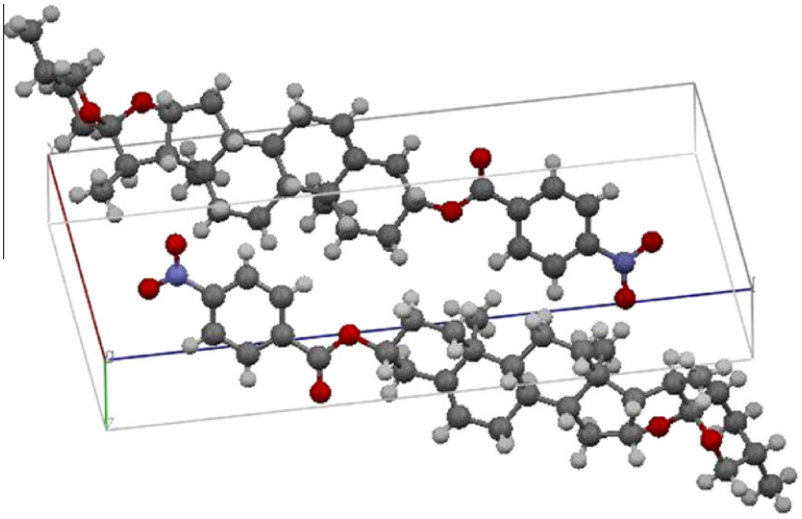

Fig. 5. Molecular diagram for unit cell of compound **2**.

is 155.90°. Molecules in the unit cell are packed together to form well-defined layers. Molecules within the layers are arranged in an antiparallel manner (Fig. 5).

3.3. Anti-adipogenic activity

The anti-adipogenic activity is shown in Fig. 6. Cell viability was measured after 2 days of incubation using MTT assay. As illustrated in Fig. 6a. compounds **1** and **2** (treatment group) in the concentration range tested (5 μM/10 μM) did not exhibit cytotoxicity, and moreover they did not influence the cell viability and proliferation during the preadipocytic stage. Also, treatment using control group (0.1% DMSO) showed similar results. The compounds **1** and **2** were also investigated for their effect on 3T3-L1 preadipocytes differentiation as shown in Fig. 6b. Both the compounds showed mild reduction of adipogenesis of 3T3-L1 preadipocytes. As displayed by Oil red O staining in Fig. 6c, cells of control group/vehicle group had accumulated lipid droplets by end of 3T3-L1 preadipocytes differentiation. On addition of compounds **1** and **2** at concentrations 5 μM/10 μM decrease in lipid accumulation was observed with fewer number of lipid cells visible. The compounds **1** and **2** (treatment group), were also tested for dose dependent inhibitory effect on TG concentration in adipocytes, both the compounds at 10 μM concentration showed a decrease in TG levels as compared to the control group Fig. 6d.

3.4. Spectral analysis

The molecular conformation obtained from crystalline structure, as well as the one yielded by geometry optimization, exhibits no special symmetries and hence the molecule belongs to C_1 point group. As a consequence, all the fundamental vibrations of free molecule are both IR and Raman active.

3.4.1. IR spectrum assignments

The correlation graph between experimental and theoretical IR wavenumbers is given in Supplementary Fig. 2. Few selected (calculated and experimental) vibrational wavenumbers (in cm^{-1}) with their assignments are given in Table 4. The total number of atoms in compound **2** is 86; hence it should give 252 ($3n - 6$) normal vibrational modes. The calculated vibrational wavenumbers are however much higher than the experimental wavenumbers due to discard of anharmonicity present in real system. The aromatic C—H stretching is observed at 3076.8 cm^{-1} in experimental IR, which closely relates to the calculated value 3050 cm^{-1}. The CH_3 stretching vibration is observed at 2922.6 cm^{-1} while the calculated is observed at 2997 cm^{-1} [35]. The C=C stretching of the olefin and aromatic are observed at 1608 and 1451.9 cm^{-1} which is in close agreement with calculated values at 1612 and 1446 cm^{1}. Ester carbonyl stretching was calculated at 1726 cm^{-1} and the corresponding absorption band was observed at

Table 4
Experimental and selected theoretical vibrational wavenumbers (cm^{-1}) of compound **2**.

Experimental	Calculated	Assignment
3076.8	3099.5	Aromatic C—H stretching
2922.6	2997.1	Aliphatic C—H stretching
2874.7	2759.3	Aliphatic C—H stretching
2363.5		Overtone of C—O stretching 6-membered ring
	2215.8	
2163.8		Overtone of C—H in plane bending vibration of 1055.2 cm^{-1}
1724.7	1726.9	C=O stretching
1608.0	1612.7	Aliphatic C=C stretching
1528.6	1534.3	Asymmetric NO_2 stretching
1451.9	1445.9	Aromatic C=C stretching
	1409.0	
1345.9	1341.4	Symmetric NO_2 stretching
	1331.1	
1278.9	1285.9	C—O stretching
	1247.5	
1217.7	1231.3	C—O stretching 5-membered ring
1174.9	1157.8	C—O stretching 6-membered ring
1055.2	1019.4	C—H in plane bending vibration of aromatic
978.6	975.7	C—H out of plane bending vibration
841.0	843.8	p-Disubstituted (aromatic)
764.8	723.7	CH_2 rocking

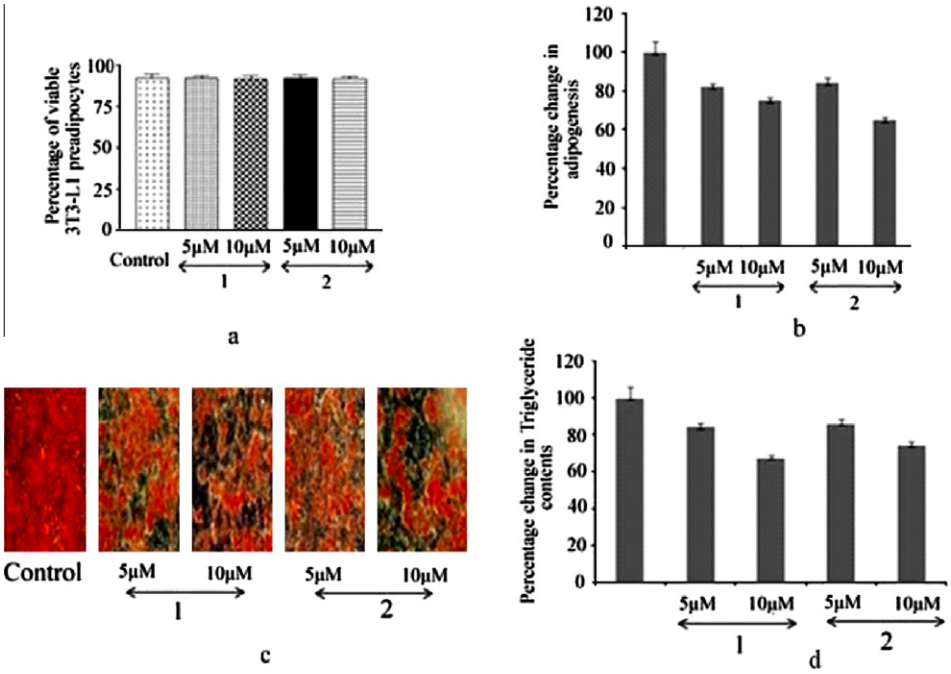

Fig. 6. Graphical representation of cytotoxicity and anti-adipogenic activity of compounds **1** and **2**.

Table 5
Experimental and calculated GIAO ^{1}H NMR chemical shifts (ppm) for compound **2** using DFT/B3LYP/6-31G(d,p).

Atom no.	Experimental chemical shift	Calculated chemical shift
H-4′	8.22	8.93
H-6′		
H-3′	8.27	8.71
H-7′		
H-6	5.44	6.17
H-3	4.93–4.88	5.31
H-16	4.46–4.38	4.05
H-26A	3.49–3.34	4.03–3.91
H-26B		
H-4A	2.50–2.47	3.01–2.41
H-4B		
H-20		
H-7A	2.04–1.96	2.27–2.01
H-7B		
H-17		
H-2A	1.90–1.79	2.01–1.83
H-2B		
H-24A		
H-24B		
H-25		
H-8	1.69–1.41	1.72–1.43
H-9		
H-11A		
H-11B		
H-12A		
H-12B		
H-14		
H-15A		
H-15B		
H-22		
H-23A		
H-23B		
H-19A	1.31	
H-19B		
H-19C		
H-18A	1.29	1.27–0.91
H-18B		
H-18C		
H-21A	0.96	1.27–0.91
H-21B		
H-21C		
H-27A	0.78	
H-27B		
H-27C		

Table 6
Experimental and calculated ^{13}C NMR chemical shifts (ppm) for compound **2** using DFT/B3LYP/6-31G(d,p).

Atom no.	δexp.	δcalcd.
C1′	164.06	152.84
C2′	136.18	132.38
C3′ + C7′	130.65	127.15 (C7′)
		125.03 (C3′)
C5′	150.44	143.72
C6′ + C4′	122.90	119.81
C1	32.06	39.53
C2	27.76	30.12
C3	75.70	73.70
C4	36.92	40.25
C5	139.28	135.96
C6	123.45	121.87
C7	32.06	34.81
C8	31.84	34.81
C9	49.94	52.79
C10	39.70	42.54
C11	20.84	24.33
C12	38.06	42.21
C13	40.26	45.15
C14	56.42	58.72
C15	31.40	34.52
C16	80.78	80.57
C17	62.08	64.85
C18	16.28	18.13
C19	19.36	21.10
C20	41.61	45.57
C21	14.52	17.27
C22	109.28	106.68
C23	31.38	33.59
C24	28.80	30.69
C25	30.29	32.86
C26	66.84	65.68
C27	17.13	19.02

1727.7 cm^{-1}. The C—O stretching vibration of ester group was observed at 1278.9 cm^{-1} which correspond to calculated value at 1285 cm^{-1}. The C—O stretching vibrations of five and six membered ring are observed in FT-IR spectrum at 1217.6 and 1174.9 cm^{-1} which closely correlate with the calculated values at 1231 and 1157 cm^{-1}. An asymmetric stretching and symmetric vibrations of the nitro function of compound **2** was observed at 1528.6 cm^{-1} and 1346 cm^{-1} respectively, which is in well agreement with theoretically computed value observed at 1534 cm^{-1} and 1331 cm^{-1} respectively.

3.4.2. NMR spectroscopy

The experimental and calculated values of ^{1}H and ^{13}C NMR chemical shifts of the title compound **2** are given in Tables 5 and 6 respectively. The carbon NMR spectrum shows only 33 peaks of different intensities, while 35 are present in the molecular formula. This suggests the presence of symmetry, as a result of which 3′, 7′ and 4′, 6′ carbon atoms are equivalent. Thirty three carbon peaks in the molecule are observed from 164.06 to 14.23 ppm in the ^{13}C NMR spectra whereas the calculated values are from 152.84 to 17.27 ppm. The agreement between calculated [GIAO B3LYP/6-31G(d,p)] and experimental data is reasonable, justifying the use of this level of theory in the prediction of the chemical shifts of the investigated compound **2**. The structure of the title compound **2** was further confirmed by 2D NMR.

3.4.3. UV–Vis absorption spectra

Compound **2** shows one strong absorption in the UV–Vis spectrum due to $\pi \rightarrow \pi^*$ transition (Supplementary Fig. 3). On the basis of fully optimized ground state structure, TD-DFT/B3LYP/6-31G(d,p) calculation have been used to determine the lowering excited state of compound **2**. The TD-DFT calculation predicts two electronic transitions at λ_{max} = 336 nm, f = 0.0082, λ_{max} = 284 nm, f = 0.0002 compared to the experimental values λ_{max} 352 and 312 nm respectively. Observed and calculated electronic transitions of high oscillatory strengths are given in Table 7. The molecular orbital plot of compound **2** is shown in Fig. 7. Highest occupied molecular orbital (HOMO) and lowest unoccupied molecular orbital (LUMO) are very popular quantum chemical parameters for predicting the chemical reactivity of the compounds. The HOMO energy characterizes the electron donating ability whereas the LUMO characterizes the electron accepting ability, and the gap between HOMO and LUMO thus characterizes the molecular chemical stability index [36].

The energy gap between HOMO and LUMO is a critical parameter in determining the molecular electrical transport property because it is a measure of electron conductivity. The HOMO of compound **2** presents a charge density localized on nitro group, whereas LUMO is characterized by charge distribution on all the carbon atoms of aromatic ring including the nitro group as well as on carbonyl group of ester. HOMO-6 however show charge density distribution around carbon atoms of aromatic ring as well as carbon–carbon double bond of ring B.

Table 7
Experimental and theoretical UV spectral parameters of compound **2**.

No.	Electronic transitions	E (eV)	Oscillatory strength (f)	Calculated (λ_{max})	Observed (λ_{max})	Assignment
1.	H → L	3.6857	0.0082	336.39	352	$\pi \rightarrow \pi^*$
2.	H-6 → L	4.3572	0.0002	284.55	312	$n \rightarrow \pi^*$

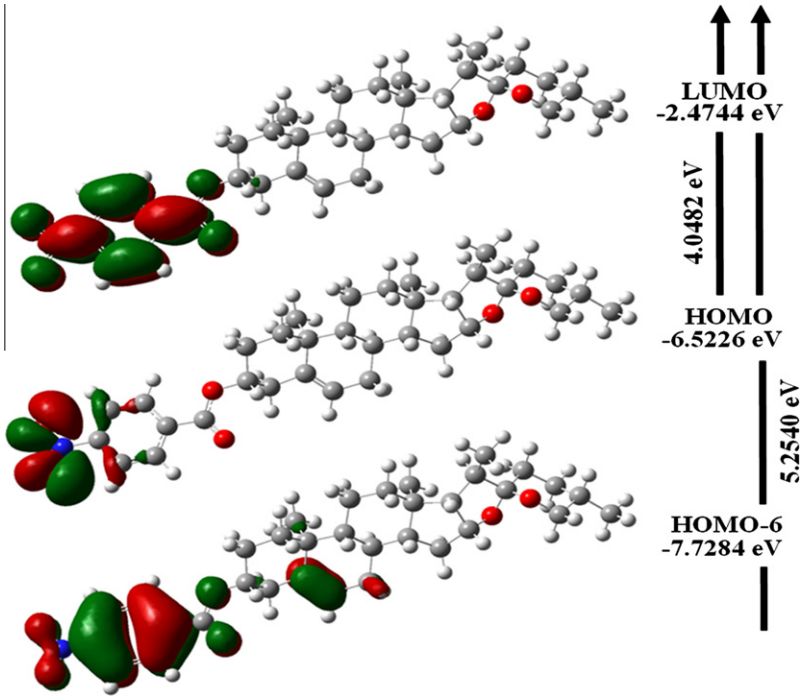

Fig. 7. HOMO–LUMO molecular plot of compound **2**.

4. Conclusion

A new synthetic compound diosgenin *p*-nitro benzoate (**2**) has been synthesized in quantitative yield by Steglich esterification in which the spiro ring remains intact. The title compound, which was characterized and studied by X-ray single crystallography, FT-IR, ^{1}H, ^{13}C NMR, 2D NMR and UV–Vis spectroscopic analysis, showed anti-adipogenic activity.

Acknowledgement

Financial assistance in the form of fellowship from Jawaharlal Nehru Fellowship program is gratefully acknowledged by Ms. Akriti Bhatia.

Appendix A. Supplementary material

The supplementary information contains images of ^{1}H (Supplementary Fig. 5), ^{13}C NMR (Supplementary Fig. 6), 2D spectra (Supplementary Fig. 7) and UV spectra (Supplementary Fig. 3) of the compound **2**. Also figures showing comparison of experimental and optimized structure, IR correlation graph, and molecular electrostatic potential diagram has been included as supplementary data. The values for calculated Cartesian atomic coordinates is also given. All other information about the crystal of the title compound **2** can be obtained in the form of supplementary crystallographic data deposited with the Cambridge Crystallographic Centre under the deposition number 854729. Supplementary data associated with this article can be found, in the online version, at http://dx.doi.org/10.1016/j.molstruc.2012.05.057.

References

[1] M. Aradhana, A.C. Rao, R.K. Kale, Int. J. Exp. Biol. 30 (1992) 367–370.
[2] R.E. Marker, J. Krueger, J. Am. Chem. Soc. 62 (1940) 3349–3350.
[3] C. Djerassi, Steroids 57 (1992) 631–641.
[4] P. Trouillas, C. Corbiere, B. Liagre, J.L. Duroux, J.L. Banaytout, Bioog. Med. Chem. 13 (2005) 1141–1149.
[5] B. Liagre, P. Vergne-Salle, C. Corbiere, J.L. Charissoux, J.L. Beneytout, Arthritis. Res. Ther. 6 (2004) R373–R383.
[6] G. Alvarez, A. Pabon, J. Carmona, S. Blair, Pytother. Res. 18 (2004) 845–848.
[7] M.J. Liu, Z. Wang, Y. Zu, R. Wong, Q.Y. Wu, Cancer Chemother. Pharmacol. 55 (2005) 79–90.
[8] J. Raju, J.M. Patlolla, M.V. Swamy, C.V. Rao, Cancer Epidemiol. Biomark. Prev. 13 (2004) 1392–1398.
[9] C. Corbiere, B. Liagre, A. Bianchi, K. Bordji, M. Dauca, Int. J. Oncol. 22 (2003) 899–905.
[10] M.J. Liu, Z. Wang, Y. Ju, R.N. Wong, Q.Y. Wu, Cancer Chemother. Pharmacol. 55 (2005) 79–90.
[11] D.Y. Leger, B. Liagre, P.J. Cardot, J.L. Beneytout, S. Battu, Anal. Biochem. 335 (2004) 267–278.
[12] S. Srinivasan, S. Koduru, R. Kumar, G. Venguswamy, N. Kyprianou, Int. J. Cancer 125 (2009) 961–967.
[13] F. Li, P.P. Fernandez, P. Rajendran, K.M. Hui, G. Sethi, Cancer Lett. 292 (2010) 197–207.
[14] J. Laguna, A. Gomez-Puyou, A. Pena, J. Guzman-Garcia, J. Atheroscler. Res. 2 (1962) 459–470.
[15] M.A. Mcanuff, W. W Harding, F.O. Omuruyi, H. Jacobs, E. Y Morrison, Food Chem. Toxicol. 43 (2005) 1667–1672.
[16] M.A. Juarez-Oropeza, J.C. Diaz-Zagoya, J.L. Rabinowitz, Int. J. Biochem. 19 (1987) 679–683.
[17] C.S. Kwon, H.Y. Sohn, S.H. Kim, J.H. Kim, K.H. Son, Biosci. Biotechnol. Biochem. 67 (2003) 1451–1456.
[18] A. Sethi, G. Bhatia, A.K. Khanna, M.M. Khan, A. Bishnoi, A.K. Pandey, A. Maurya, Med. Chem. Res. 20 (2011) 36–46.
[19] B. Neises, W. Steglich, Angew. Chem. Int. Ed. 17 (1978) 522–524.

[20] SAINT+ 6.02 ed.; Bruker AXS; Madison, WI, 1999.
[21] L.J. Farrugia, J. Appl. Crystallogr. 32 (1999) 837–838.
[22] G.M. Sheldric, Acta Crystallogr. A64 (2008) 112–122.
[23] A.L. Spek, J. Appl. Crystallogr. 36 (2003) 7–13.
[24] M.N. Burnett, C.K. Johnson, ORTEP-III: Oak Ridge Thermal Ellipsoid Plot 318 Program for Crystal Structure Illustrations, Report ORNL-6895, Oak Ridge 319 National Laboratory, Oak Ridge, TN, USA, 1996.
[25] J. Folch, M. Lees, G.H.S. Stanley, J. Biol. Chem. 226 (1957) 497.
[26] K.N. Frayn, P.F. Maycock, J. Lipid Res. 21 (1980) 139–144.
[27] M.J. Frisch, G.W. Trucks, H.B. Schlegel, G.E. Scuseria, M.A. Robb, J.R. Cheeseman, J.A. Montgomery Jr., T. Vreven, K.N. Kudin, J.C. Burant, J.M. Millam, S.S. Iyengar, J. Tomasi, V. Barone, B. Mennucci, M. Cossi, G. Scalmani, N. Rega, G.A. Petersson, H. Nakatsuji, M. Hada, M. Ehara, K. Toyota, R. Fukuda, J. Hasegawa, M. Ishida, T. Nakajima, Y. Honda, O. Kitao, H. Nakai, M. Klene, X. Li, J.E. Knox, H.P. Hratchian, J.B. Cross, V. Bakken, C. Adamo, J. Jaramillo, R. Gomperts, R.E. Stratmann, O. Yazyev, A.J. Austin, R. Cammi, C. Pomelli, J.W. Ochterski, P.Y. Ayala, K. Voth, G.A. Morokuma, P. Salvador, J.J. Dannenberg, V.G. Zakrzewski, S. Dapprich, A.D. Daniels, M.C. Strain, O. Farkas, D.K. Malick, A.D. Rabuck, K. Raghavachari, J.B. Foresman, J.V. Ortiz, Q. Cui, A.G. Baboul, S. Clifford, J. Cioslowski, B.B. Stefanov, G. Liu, A. Liashenko, P. Piskorz, I. Komaromi, R.L. Martin, D.J. Fox, T. Keith, M.A. Al-Laham, C.Y. Peng, A. Nanayakkara, M. Challacombe, P.M.W. Gill, B. Johnson, W. Chen, Wong, M.W. Wong, C. Gonzalez, J.A. Pople, Gaussian 03, Revision C.02, Gaussian Inc., Wallingford, CT, 2004.
[28] A.D. Becke, J. Chem. Phys. 98 (1993) 5648–5652.
[29] N. Sundaraganesan, E. Kavitha, S. Sebastian, J.P. Cornard, M. Martel, Spectrochim. Acta Part A Mol. Biomol. Spectrosc. 74 (2009) 788–797.
[30] G.A. Zhurko, D.A. Zhurko, Chemcraft: Lite Version Build 08 (Freeware), 2005.
[31] Computer program Gauss View 3.09, Ver. 2, Gaussian, Inc., PA. Pittsburgh.
[32] S.J. Grabowski, A.T. Dubis, J. Phys. Chem. A 108 (2004) 5815–5822.
[33] P.E. Oscar, C.E. Edurado, Z.T.E. Gloria, T.B. Silvia, B.J. Enrique, Z. Naturforsch. 57c (2002) 947–950.
[34] H.N. De Armas, N.M. Blaton, O.M. Peeters, C.J. De Ranter, R.P. Hernandez, M.A.I. Arteagas, R.P. Gil, F.C. Manchado, Acta Crystallogr. C55 (1999) 601.
[35] G. Varsanyi, Assignments for Vibrational Spectra of Seven Hundred Benzene Derivatives, vol. 1–2, Adam Hilger, 1974.
[36] S.W. Xia, X. Xu, Y.L. Sun, Y.L. Fan, Y.H. Fan, C.F. Bi, D.M. Zhang, L.R. Yang, China J. Struct. Chem. 25 (2006) 849–853.